Radiocarbon Dating of the Nyixoi Chongco Rock Avalanche, Southern Tibet: Search for Signals of Seismic Shaking and Hydroclimatic Events

Guanghao Ha[1,2], Feng Liu[3]*, Maotang Cai[3], Junling Pei[3], Xin Yao[3] and Lingjing Li[3]

[1]Key Laboratory of Seismic and Volcanic Hazards, Institute of Geology, China Earthquake Administration, Beijing, China, [2]Institute of Geology, China Earthquake Administration, Beijing, China, [3]Institute of Geomechanics, Chinese Academy of Geological Sciences, Beijing, China

Landslides are important agents of the surface processes involved in the growth of mountainous topography. Dating prehistoric landslides is a prerequisite for establishing the relationships between prehistoric slope instability, and past climatic regimes and paleoseismic records. The Nyixoi Chongco rock avalanche (NCRA) is located in the Angang graben within the N–S trending rift zone in southern Tibet. It represents a giant prehistoric mass wasting event that was characterized by exceptional mobility and a large volume. However, the exact emplacement time and origin of the NCRA are still controversial. In this study, we conducted ^{14}C dating of peat layers and snail shells to constrain the emplacement age of the NCRA. The ^{14}C ages of the organic material and plant remnants in the basal peat layer are 1272–1389 and 1299–1404 cal AD, respectively. The ^{14}C ages of aquatic snail shells and the bog overlying the rock avalanche are 425–565 and 1022–159 cal AD, respectively. These results indicate that the NCRA consisted of at least two separate and distinct events, instead of the single event suggested by previous studies. Based on field investigations and temporal correlations, we infer that there may be no paleoseismic records in the Angang graben that would corroborate a coseismic trigger for the NCRA. Therefore, we suggest that the ^{14}C ages of the sediments below and above the landslide rocks should be interpreted carefully. The ^{14}C ages alone do not provide sufficient evidence to infer the true trigger of the NCRA event.

Keywords: Nyixoi Chongco rock avalanche, Angang graben, southern Tibet, ^{14}C dating, earthquake, climate change

INTRODUCTION

Rock avalanches are the result of the detachment of large volumes (>1 Mm^3) of intact rock during extremely rapid, massive flow-like movements (Hungr et al., 2001). Due to their high velocities, large dimensions, and long run-out distances (Sembroni et al., 2019), rock avalanches are one of the major agents of hillslope erosion and pose a threat to property in mountain ranges. Reconstructing the occurrence history of rock avalanches is a key issue in discerning whether an increased incidence of such events can be expected in the future. To answer this question, it is important to identify the timing of past rock avalanche events and to correlate them with reconstructed seismic and/or climatic records.
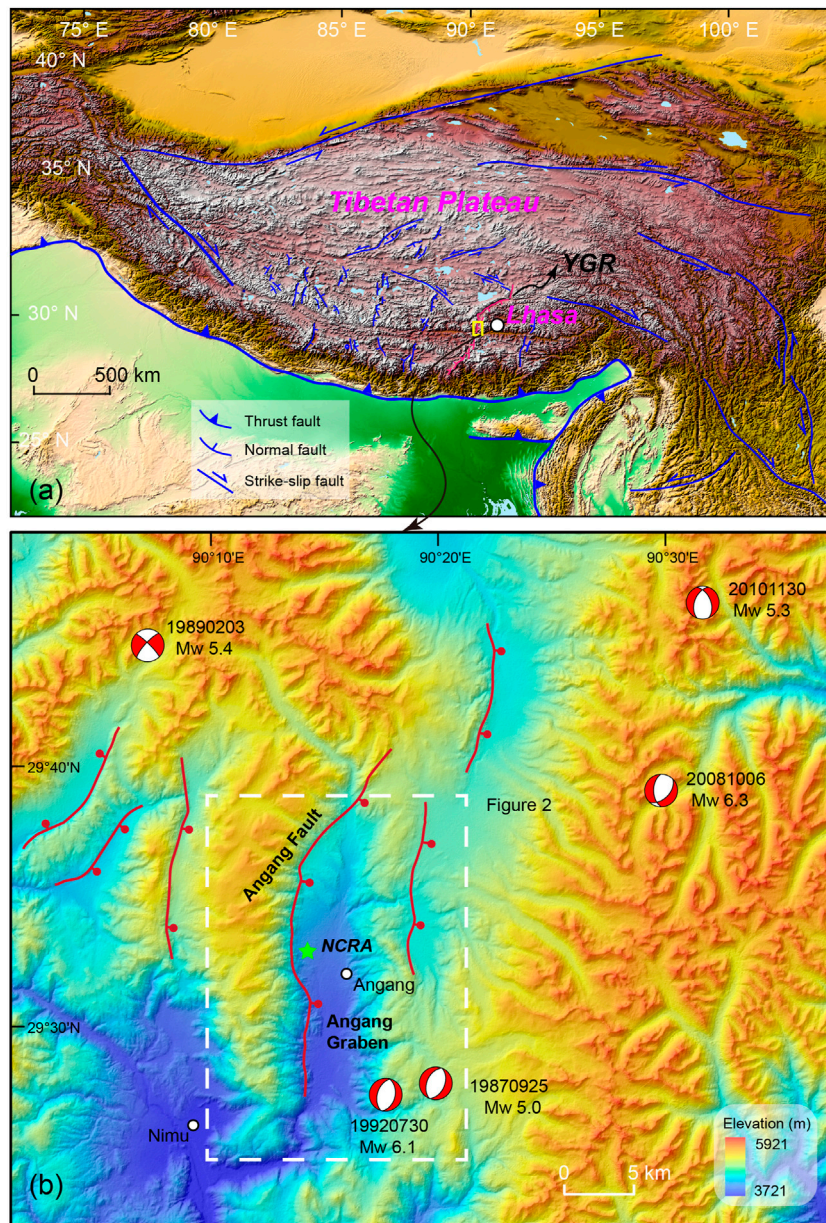
FIGURE 1 | (A) Simple tectonic map of the Tibetan Plateau. The pink fault line is the Yadong–Gulu rift (YGR). **(B)** The Nyixoi Chongco rock avalanche (NCRA) is located on the western side of the Angang graben. The focal mechanism solution data are from website https://www.globalcmt.org/CMTsearch.html (Accessed July 9, 2020).

The Nyixoi Chongco rock avalanche (NCRA) is located in the Angang graben in the middle segment of the Yadong–Gulu Rift (YGR), southern Tibet (**Figure 1**). It is considered to be the product of a large earthquake event (Wu et al., 2015; Zeng et al., 2020). However, preconditioned slopes may fail as a result of a number of factors (e.g., earthquakes, glacial events, and heavy rainfall) (Mitchell et al., 2007; Korup et al., 2013). Establishing a connection between paleolandslides and triggers is based on landslide ages (Struble et al., 2020). If a synchrony among landslide events can be identified, the mechanisms of paleolandslides can be inferred to be seismic or extreme

hydrologic events (Pánek, 2015). However, the age of the NCRA is still controversial. The NCRA has been inferred to have occurred during the latest tectonic event (strong seismic event) on the normal fault bounding the Angang graben at 2.4 ± 0.2 ka based on the optically stimulated luminescence (OSL) age of the normal fault–scarp colluvium (Wu et al., 2015). Zeng et al. (2020) reported a ^{14}C age of 820 ± 30 years BP ($1,220 \pm 30$ years cal AD) for the NCRA, which was dated from a humus substrate. A correlation between the NCRA and the Chubusi earthquake (1264 AD), which occurred outside the Angang graben, was simply proposed (Zeng et al., 2020).
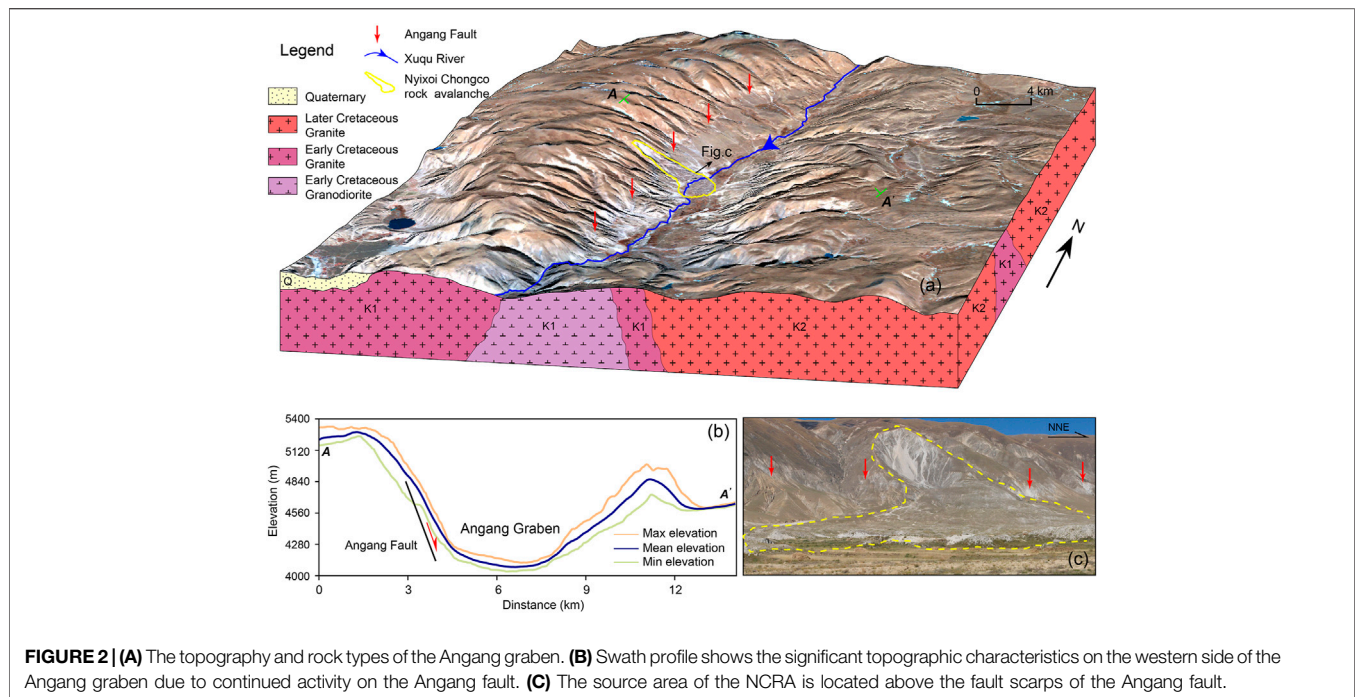
FIGURE 2 | (A) The topography and rock types of the Angang graben. **(B)** Swath profile shows the significant topographic characteristics on the western side of the Angang graben due to continued activity on the Angang fault. **(C)** The source area of the NCRA is located above the fault scarps of the Angang fault.

However, it should be noted that Zeng et al. (2020) only provided a single radiocarbon age for a bulk organic sample and misinterpreted the upper age as the event age of the NCRA. In this study, we determined the occurrence time of the NCRA using ^{14}C ages of plant remains and snail shells. Based on these new ^{14}C ages, high-resolution aerial images, and field observations, we reinterpreted the landslide event associated with the NCRA. Furthermore, the limitations of using ^{14}C dating alone to determine the occurrence time of the NCRA are also discussed in this paper. The uncertainty of the potential triggering factors of the NCRA are also discussed in the context of the regional tectonics and paleoclimate.
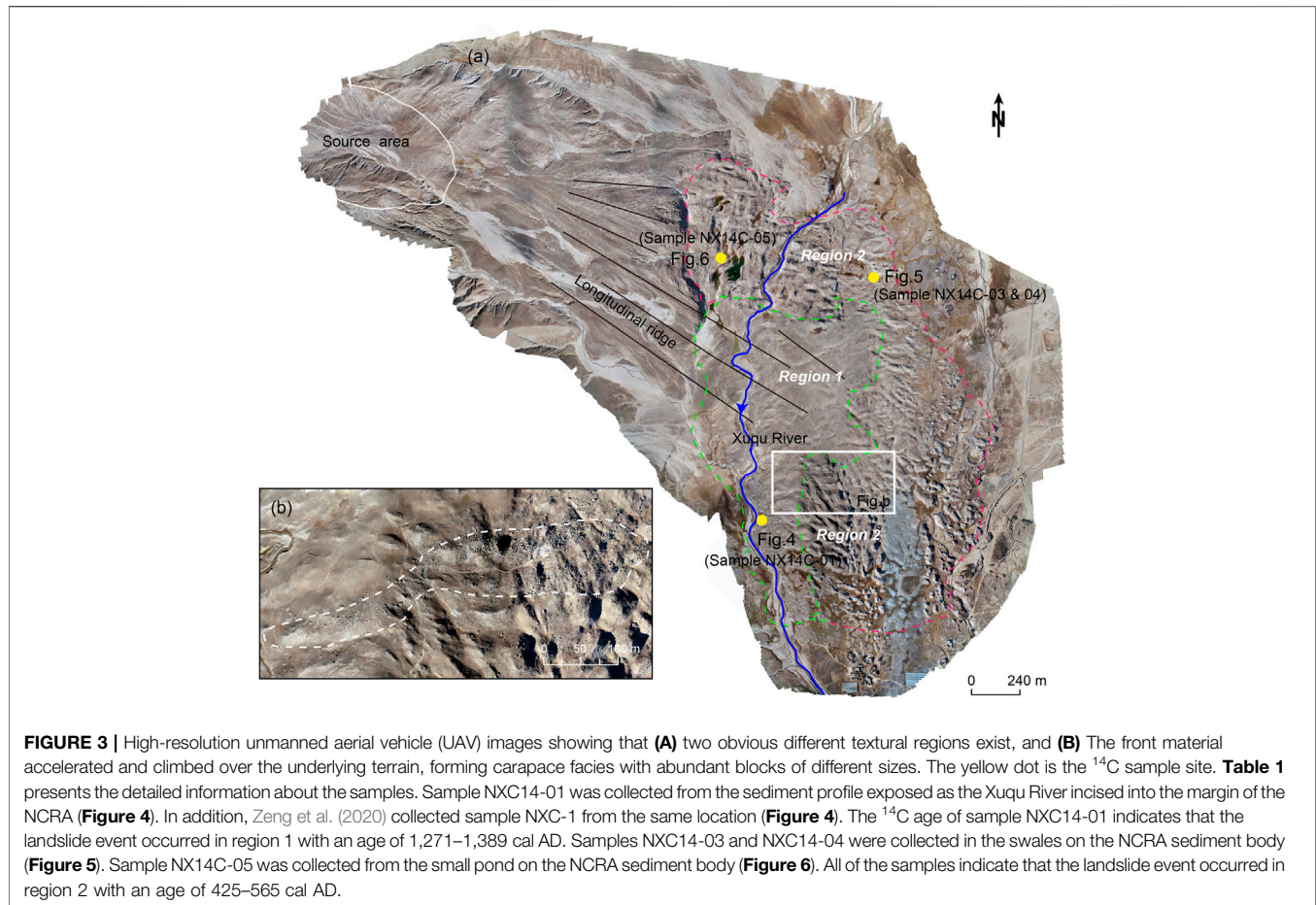
GEOLOGIC AND GEOMORPHIC SETTING

The Neogene rift system, which is characterized by a series of N–S trending grabens in southern Tibet, is considered to be one of the most prominent structures caused by the continuous post-collision intracontinental convergence between India and Eurasia (Yin and Harrison, 2000). The YGR is the most significant and youngest rift (Harrison et al., 1995; Chung et al., 2005; Mahéo et al., 2007), and it is the longest one within the Tibetan Plateau, extending for over 500 km from Yadong to Gulu (**Figure 1A**) (Armijo et al., 1986).

According to the geometry and kinematic indicators of its boundary faults, the YGR can be divided into three segments: the northern, central, and southern segments (Armijo et al., 1986; Ha et al., 2019). The NCRA occurred on the western side of the Angang graben in the central segment of the YGR (**Figure 1B**). In this segment, the Angang graben is bounded by a pair of normal faults on both sides of the rift (Armijo

et al., 1986). However, some researchers have argued about the existence of the eastern boundary normal fault of the Angang graben (Wu et al., 2015). In contrast, the western boundary normal faults, namely, the Angang Fault (Armijo et al., 1986) and Nimu Fault (Zeng et al., 2020), are easy to recognize both in the field and on satellite images due to a clear fault plane and linear fault scarp trace, respectively. The topographic relief of the western slope is steeper and higher than that of the eastern slope, with a series of typical tectono-geomorphic indicators, including fault scarps, colluvial wedges, and deformed fluvial terraces (**Figure 2B**). A previous study reported a vertical movement rate of 0.8–1.3 mm a^{-1} on the Angang Fault since 26 to 23 ka (Wu et al., 2015). Along this fault, six large paleo-earthquakes have been identified, with the last two seismic events occurring at 5.8 ± 1.0 and 2.4 ± 0.2 ka (Wu et al., 2015). The lithology within the Angang graben is dominated by Miocene monzonitic granite with a U–Pb zircon age of ~15 Ma (Ji et al., 2009), which constitutes the bedrock of the high topography on both shoulders of the graben (**Figure 2A**). The continued activity along the active Angang Fault has resulted in a wide fault zone. The granite that outcrops along the fault trace has been intensively fractured and weathered.

The NCRA included an initial rock slope failure with a mass of 2.8 × 10^7 m^3, which traveled ~4.6 km down slope, with a vertical distance of 885 m (Wang et al., 2019a). The NCRA dammed the Xuqu River flow across the Angang graben. The bedrock of the source is composed of granite. The intensively fractured granite with a series of joints and fissures can be observed in the field. Two dominant sets can be traced, which substantially weakened the granite and controlled wedge failures in the source area (Wang et al., 2019a). The NCRA is characterized by complex surface landforms (e.g., Toreva blocks, longitudinal and transverse ridges, *en echelon* ridges,

FIGURE 3 | High-resolution unmanned aerial vehicle (UAV) images showing that **(A)** two obvious different textural regions exist, and **(B)** The front material accelerated and climbed over the underlying terrain, forming carapace facies with abundant blocks of different sizes. The yellow dot is the ^{14}C sample site. **Table 1** presents the detailed information about the samples. Sample NXC14-01 was collected from the sediment profile exposed as the Xuqu River incised into the margin of the NCRA (**Figure 4**). In addition, Zeng et al. (2020) collected sample NXC-1 from the same location (**Figure 4**). The ^{14}C age of sample NXC14-01 indicates that the landslide event occurred in region 1 with an age of 1,271–1,389 cal AD. Samples NXC14-03 and NXC14-04 were collected in the swales on the NCRA sediment body (**Figure 5**). Sample NX14C-05 was collected from the small pond on the NCRA sediment body (**Figure 6**). All of the samples indicate that the landslide event occurred in region 2 with an age of 425–565 cal AD.
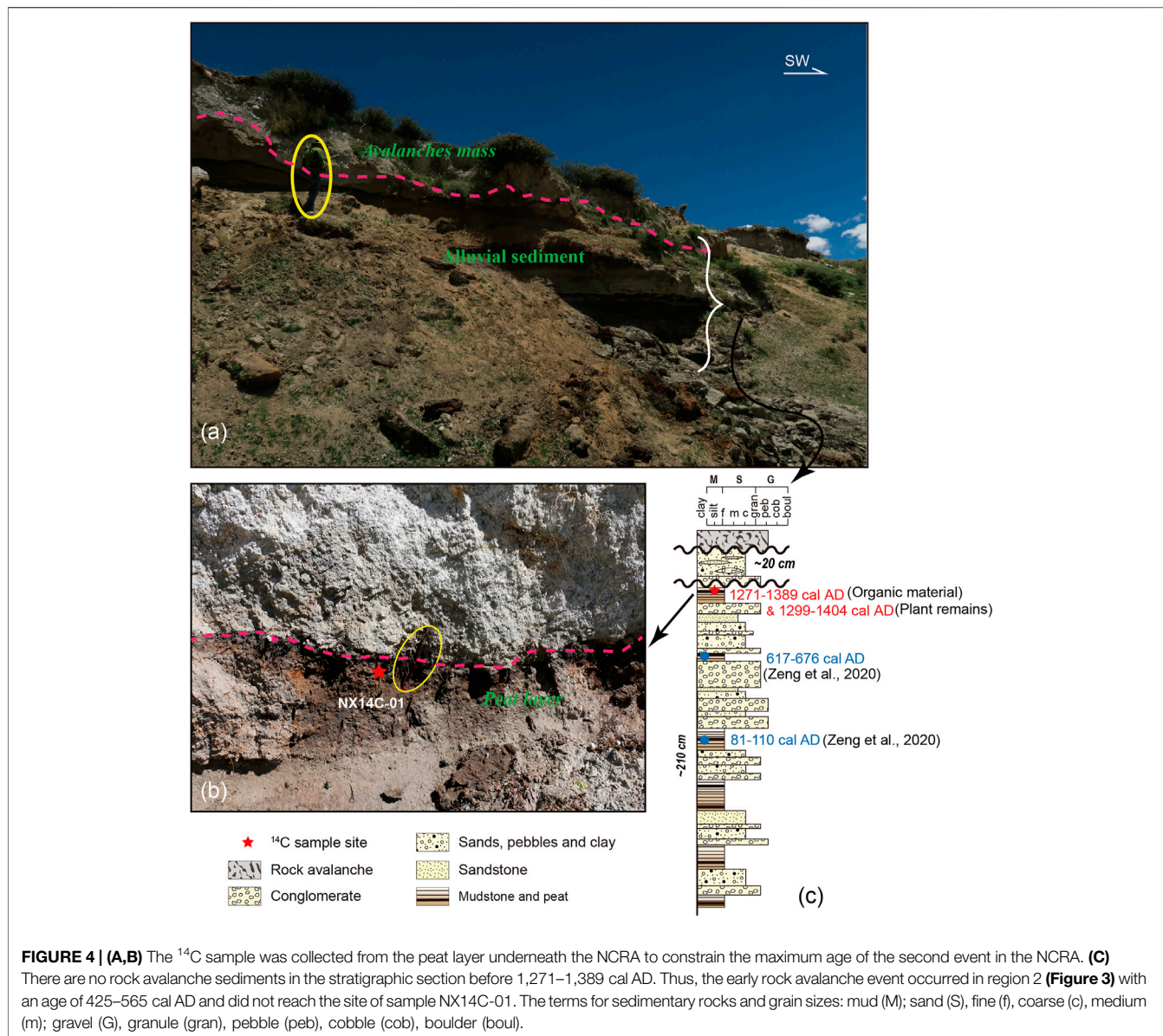
and hummocks) and internal sedimentary structures (e.g., jigsaw structures, inner-shear zones, aligned clasts, diapiric structures, and convoluted structures), implying a rapid stacking process, which is similar to laminar flow transport (Wang et al., 2019b). A small lake and pond have developed within depressions above the chaotic rock avalanche deposit, providing critical lacustrine sediments to constrain the minimum age of the NCRA (**Figure 3A**). The western slope has experienced more severe erosion than the eastern slope due to the extensive development of glaciers in the Quaternary (Wu et al., 2015). However, the precise time at which the glaciation took place is still unknown. The glacier is no longer present, and this area is only covered with snow in winter. The present average annual air temperature is around 7°C, and the average annual precipitation is 340 mm from 1971 to 2000 (available at http://data.cma.cn/).

METHODS

As the Xuqu River incised the rock avalanche deposit, the sample profile was exposed on the margin of the NCRA (**Figure 3**). In this study, sample NX14C-01 was collected from a 5-cm-thick peat layer underlying the rock avalanche

mass (**Figure 4**) (Zeng et al., 2020). The plant remnants were picked from sample NX14C-01 to conduct ^{14}C dating. In addition, the organic material separated from this sample was also dated using the ^{14}C method to evaluate the potential old carbon effect on this sample. There are abundant small lakes, ponds, and wetlands that formed in the small intervening internally drained swales between the hummocks on the surface of the NCRA (**Figures 5**, **6**). A pit was dug from the surface down to the rock avalanche material, and snails and plant remnants were sampled for radiocarbon dating (**Figure 5**). Sample NX14C-05 was collected from a small pond, and the organic material was picked out for dating (**Figure 6**).

All of the samples were pretreated and dated in the Beta Analytic lab in the United States using accelerator mass spectrometry (AMS). The raw ^{14}C dates were converted into calendar ages using the IntCal 20 calibration curve (Reimer et al., 2020) in the OxCal v4.4.2 software. In this paper, the calibrated ages are expressed as their two-sigma ranges. In addition, Zeng et al. (2020) reported a ^{14}C age with a one-sigma range. In order to determine the difference in the ^{14}C ages of the organic sediment and plant remains, we recalibrated the ^{14}C age of the dry humus sample of Zeng et al. (2020) using the same calibration curve and software.

FIGURE 4 | (A,B) The ^{14}C sample was collected from the peat layer underneath the NCRA to constrain the maximum age of the second event in the NCRA. **(C)** There are no rock avalanche sediments in the stratigraphic section before 1,271–1,389 cal AD. Thus, the early rock avalanche event occurred in region 2 **(Figure 3)** with an age of 425–565 cal AD and did not reach the site of sample NX14C-01. The terms for sedimentary rocks and grain sizes: mud (M); sand (S), fine (f), coarse (c), medium (m); gravel (G), granule (gran), pebble (peb), cobble (cob), boulder (boul).

RESULTS

The detailed descriptions and age results of the samples are presented in **Table 1**. The organic samples were collected from sediments below the landslide body. The organic materials and plant remnants were separated from sample NX14C-01, and their calibrated ^{14}C ages were determined to be 1,272–1,389 and 1,299–1,404 cal AD, respectively (**Figure 4B**). The ^{14}C ages of the humus sample is 820 ± 30 years BP (1,220 ± 30 cal AD) (Zeng et al., 2020). The new 2σ calibrated ^{14}C age range of the sample of Zeng et al. (2020) is 1,175–1,273 cal AD (**Table 2**). The ^{14}C age of the organic materials in this study are close to that of Zeng et al. (2020). In contrast, the ^{14}C age of the plant remains is younger than that of the organic materials and dry humus reported by Zeng et al. (2020).

Sediments from the swales mainly consisted of dark gray laminated organic rich peat and grayish white silt. Snails and fragments occur in the silt toward the sharp landslide contact, which is indicated by angular granite gravel (**Figure 5B**). There is no obvious change in the amount of organic matter of the peat layer. Similarly, the silt content has no significant change. It is noted that there is no fluvial or flood sediment in the swale sediment. The fine grain size of the whole sediment profile indicated that there was no large amount of rain in the study area after the emplacement of the NCRA. Otherwise, the coarse landslide debris sediment may be introduced into the swales.

Modern plants grow in the upper 3 cm of the peat, followed by gray-white lacustrine deposits, which are overlain by 45 cm of peat (**Figure 5B**). Abundant plant roots and shells are present in the peat, and the color of the plant
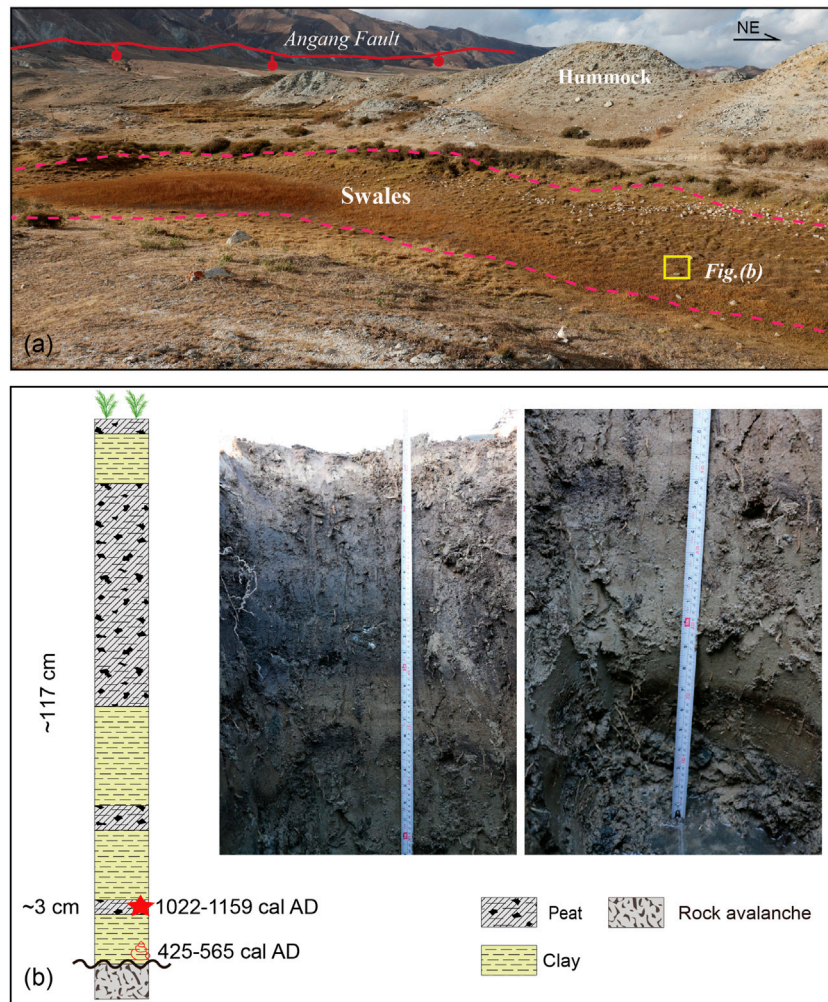
FIGURE 5 | (A) The 14C sample was collected from swales above the NCRA to constrain the minimum age of the first landslide event represented by the NCRA sediment. **(B)** Snails and plant remnants were sampled for radiocarbon dating in the sediment profile.

remains is partially yellow. The humification degree of the peat is low. The subsequent layer of lacustrine deposits is 52-cm thick and contains snail shells (**Figure 5B**). Two thin peat layers occur in the middle and bottom of the lacustrine deposit. Sample NX14C-03 is located in the second peat layer with a thickness of 3 cm, and the ^{14}C age of this layer 1 is 022–1,159 cal AD (**Figure 5B**). Snail sample NX14C-04 was collected from the bottom of the lacustrine deposit (**Figure 5B**). Its ^{14}C age is 425–565 cal AD. Below the lacustrine deposition is the NCRA sediment body.

Sample NX14C-05 was collected from a small pond. A sediment layer with a depth of 50 cm was dug in the field. This layer is characterized by medium and coarse sand-containing mud. The mud sediment was sampled for radiocarbon dating, and the age of sample NX14C-05 was determined to be 660–774 cal AD.

DISCUSSION

Two Landslide Events Occurred in the Nyixoi Chongco Rock Avalanche

According to the ^{14}C ages and sample locations (**Figures 4–6**), the NCRA may have consisted of two landslide events. The younger and older events are located in regions 1 and 2, respectively (**Figure 3A**). From the unmanned aerial vehicle (UAV) photos, two regions with different textures can be recognized. Region 1 has a smooth texture, while region 2 has a sharp texture, and there is a clear boundary between these two regions (**Figure 3A**). The NCRA sediments are mainly composed of scattered granite rocks. If there was only one event, the surface of the landslide sediments should not exhibit significant differences in texture on the images (green dotted outline in **Figure 3**) under the same climate environment. Thus, two landslide events are the simple
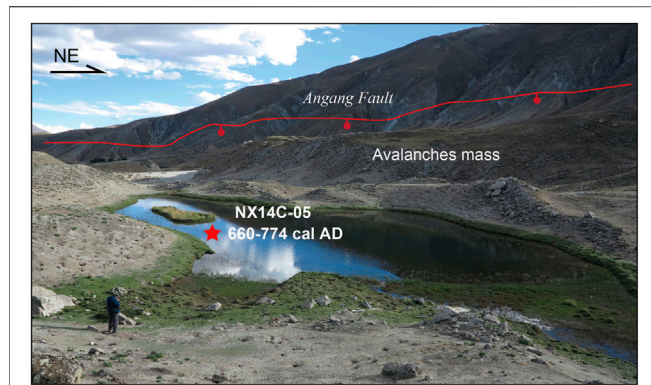
FIGURE 6 | The ^{14}C sample was collected from a small pond above the NCRA to constrain the minimum age of the first landslide event represented by the NCRA sediments.

interpretation of the different textures in the images shown in **Figure 3**. In addition, according to our observations, the different textures in the images are not caused by the Xuqu River because there are no fluvial sediments in the hummock of the landslide body. The elongated longitudinal ridges close to the source area indicate the high-velocity transport direction (Wang et al., 2019b). This region was restricted between the detached source area and the Xuqu River Valley (Wang et al., 2019). Based on the high-resolution UAV photos, the

microtopography associated with the the mass movement direction of the avalanche can be identified in region 1 (**Figure 3A**). Due to the rerouting of the Xuqu River after the emplacement of the NCRA, part of the microtopography was eroded away and became less clear. In addition, some fractured rock falls are scattered in the boundary area between regions 1 and 2 (**Figure 3B**). This suggests that the frontal mass suddenly decelerated and was rapidly ejected due to an increase in topographic undulation or increased basal friction (Wang et al., 2019b). All of these morphological and textural characteristics suggest that the NCRA sediment is the result of two rock avalanche events.

Figure 4C shows the characteristics of the depositional environments before 1,299–1,404 cal AD. The lithofacies association consists of coarse sand interbedded with a peat layer and the absence of rock avalanche sediments. This indicates that episodic contraction and expansion of the water level occurred near sample site NX14C-01 without the interruption of any rock avalanche event before 1,299–1,404 cal AD. That is, the 425–565 cal AD event occupying region 2 did not reach the site where sample NX14C-01 was collected (**Figure 3A**). Thus, **Figure 4C** shows the 1,299–1,404 cal AD rock avalanche event occupying region 1. The younger event may have been caused by reworking of the rock avalanche sediment in region 2 or by a new rock avalanche. However, we do not know the real origin of this event at present. We suggest that two landslide events may have deposited the

TABLE 1 | Radiocarbon analyses of samples.

Sample number	Lab no	13C/12C (0/00)	Radiocarbon age (year B.P. ± 1 σ)	Calibrated age (cal year A.D.)	Probability (2σ)	Material
NX14C-01	Beta-533721	−25.6	690 ± 30	1,272–1,389	95.4	Organic sediment
NX14C-01	Beta-555473	−26.5	610 ± 30	1,299–1,404	95.4	Plant remains
NX14C-03	Beta-559276	−16	970 ± 30	1,022–11,59	95.4	Plant remains
NX14C-04	Beta-557626	−7.9	1,570 ± 30	425–565	95.4	Snail
NX14C-05	Beta-533723	−21.5	1,300 ± 30	660–774	95.4	Organic sediment

Note. All of the samples were pretreated and dated by Beta Analytic Inc. using accelerator mass spectrometry (AMS). The calibrated ages with 2σ are from the online OxCal v4.4.2 software (Ramsey, 2020) and were obtained using the IntCal 20 calibration curve (Reimer et al., 2020).

TABLE 2 | Radiocarbon analyses of samples conducted in previous studies.

Sample number	Lab no	13C/^{12}C (0/00)	Radiocarbon age (year B.P. ± 1σ)	Calibrated age[a] (cal year C.E.)	Probability (1σ)[b]	New calibrated age[c] (cal year A.D.)	Material
NXC-1	XA22679	−27.9	820 ± 30	1,220 ± 30	1,194–1,196 CE/1.2% 1,206–1,259 CE/98.8%	1,175–1,273/ 95.4%	Dry humus
NXC-3D	XA22680	−26.08	1,370 ± 20	656 ± 9	650–663 CE/100%	617–676/ 95.4%	Peat within sand
NXC-7	XA22681	−27.45	1,990 ± 25	11 ± 31	21–10 BCE/15.1% 2 BCE–30 CE/55.2% 37–51 CE/20.7%	81–110/ 95.4%	Dry humus

[a]The calibrated ages with 1σ are from the online OxCal v4.3.2 software.
[b]The range/possibility values with 1σ are from the online CALIB REV7.1.0 software. The samples were tested at the Xi'an Accelerator Mass Spectrometry Center, with a half-life of 5,568 a.
[c]The calibrated ages with 2σ are from the online OxCal v4.4.2 software (Ramsey, 2020) and were obtained using the IntCal 20 calibration curve (Reimer et al., 2020). Sample NXC-1 was collected from the same location as ours (**Figure 4**).

NCRA sediments. Generally, the interpretation of radiocarbon ages as the minimum, maximum, or event age of landslides depends on whether the sampled material is located on, below, or is mixed within the landslide body (Lang et al., 1999). According to the sample locations (**Figure 4B**), the first event may have occurred in region 2 at a minimum of 425–565 cal AD. Similarly, the second one may have occurred in region 1 at a maximum of 1,299–1,404 cal AD (**Figure 5**). This may be the reason for the younger ^{14}C age of the deposits below the rock avalanche than that of the deposits above the rock avalanche (**Figures 4**, **5**).

If the NCRA only consisted of a single landslide event, the results of our ^{14}C dating of the pond sediments above the avalanche mass should be younger than that of the peat sample below. However, **Table 1** presents age results that are inconsistent with this scenario. We tend to rule out this possibility due to the following reasons. First, the hard water effect, which is the presence of calcium ions resulting from the dissolution of infinite-age calcium carbonate, can affect the ^{14}C dating of terrestrial shells (Bowman, 1990). However, there are no carbonate formations in the study area. Second, the peat sample could have a radiocarbon reservoir effect, which could result in an age that is hundreds of years older than the real age (Kilian et al., 1995; Shore et al., 1995; Nilsson et al., 2001). Therefore, dating terrestrial plant remnants using AMS is better than dating bulk sediments (Ma et al., 2009). In addition, there is about a 500-year gap between the ^{14}C age of the organic sediments located on (sample NX14C-05) and below (sample NX14C-01) the landslide body in this study (**Table 1**). In contrast, there is only a 100-year difference between the organic sediment fraction and the peat fraction in sample NX14C-01, which underlies the NCRA. It is unlikely that the old carbon effect would result in such old radiocarbon ages for the samples above the NCRA. Thus, our ages for the snail shells and plant remains cannot be denied based on a single previous ^{14}C age alone. We are inclined to believe that the NCRA sediments represent two landslide events.

Groundwater that has been isolated from the atmosphere may have introduced a significant old carbon effect (Zimmerman and Myrbo, 2015). The sample collected from the peat layer immediately underlying the NCRA body is high enough to exclude the impact of groundwater at present (Zeng et al., 2020). However, the paleohydrology of the peat deposits in the Angang graben remains unknown. Thus, the best ^{14}C sample is identifiable terrestrial well-preserved plant remnants within the peat layers (Ma et al., 2009; Piotrowska et al., 2011). Since the plant remnants have not been entirely decomposed, their age should be considered to be the real age of the peat sedimentation (Zhou et al., 2002). Thus, we suggest that the old carbon effect may have caused the ^{14}C age difference between the humus and the plant remains.

The snails were picked from the basal section of the sediments, which is mainly composed of coarse quartz sands (**Figure 5B**) that originated from the landslide body sediments and was shed from the granite. This represents the ecesis interval between the snail occurrence and the emplacement of the first event of the NCRA. Thus, the snail age provides a minimum age for the landslide event. The old carbon effect may induce an older age for sample NX14C-04. Freshwater shells commonly incorporate carbon dissolved in water rather than the atmosphere. As a result, dated shells contain a low isotopic ratio of [14]C–[12]C compared with the atmosphere and may be older (Clague, 2015). However, the uncertainties introduced by this may be minimal in this study based on our observations and the present climate. First, the snails were collected from the enclosed swales above the NCRA. Meteoric precipitation is the main water resource in this area according to field observations. The sediment records suggest that the swales probably contained standing water after movement that was immediately accompanied by deposition of clay, silt, and organic matter (**Figure 5B**). The sedimentary environment of the sample pond does not indicate fluvial input. Second, the peat sediment layer immediately underlying the NCRA sediment body is located above the groundwater and avoids carbonate contamination of the ^{14}C ages (Zeng et al., 2020). As a result, the ^{14}C age of the snails at the base of the pond deposits should yield reliable ages for the pond formation.

Possible Triggers

The NCRA has been hypothesized to have a seismic origin based on the morphology and size of the landslide (Wu et al., 2015). However, none of the morphological criteria of seismic paleolandslides are definitive. In addition to earthquakes, there are many other causes of landslides (Jibson, 2009). For example, more than 100 of the largest cluster of giant (>108 m³) slope failures mobilized along basal failure planes with gradients as low as ~5° due to oscillating sea levels in the tectonically quiescent Caspian Depression of western Kazakhstan (Pánek et al., 2016). These landslides are characterized by large volumes, sizes, and spatial clustering and occurred in a subdued landscape. The morphology of these landslides seems to meet the criteria of seismic landslides described by Wu et al. (2015), but they are nonseismic landslides (Pánek et al., 2016). Thus, the presence of independent active fault or liquefaction evidence due to paleoseismic events can be used to determine if paleolandslides have a seismic origin (Jibson, 2009). In addition, the last large paleoearthquake occurred at 2,400 ± 200 years BP based on OSL dating of the fault scarp colluvium in the Angang graben (Wu et al., 2015). Thus, the NCRA was triggered by the 2,400 ± 200 years BP seismic event (Wu et al., 2015). In addition, tying prehistoric slope instability to specific triggering events requires landslide ages. Therefore, without an age for the NCRA (Wu et al., 2015), it seems dangerous to assign a seismic trigger as its origin. Our results indicate that the first event of the NCRA may have occurred before 425–565 cal AD. If so, the large earthquakes associated with the repeated active boundary fault mentioned by Wu et al. (2015) may have served as a prelude to this landside event.

The age of the second landslide event of the NCRA is 820 ± 30 years BP (1,220 ± 30 cal AD) based on dating of the humus substrate, with a new calibrated age of 1,175–1,273 cal AD from this study, which is connected to the 1264 AD Chubusi earthquake (Zeng et al., 2020). It seems that there is a
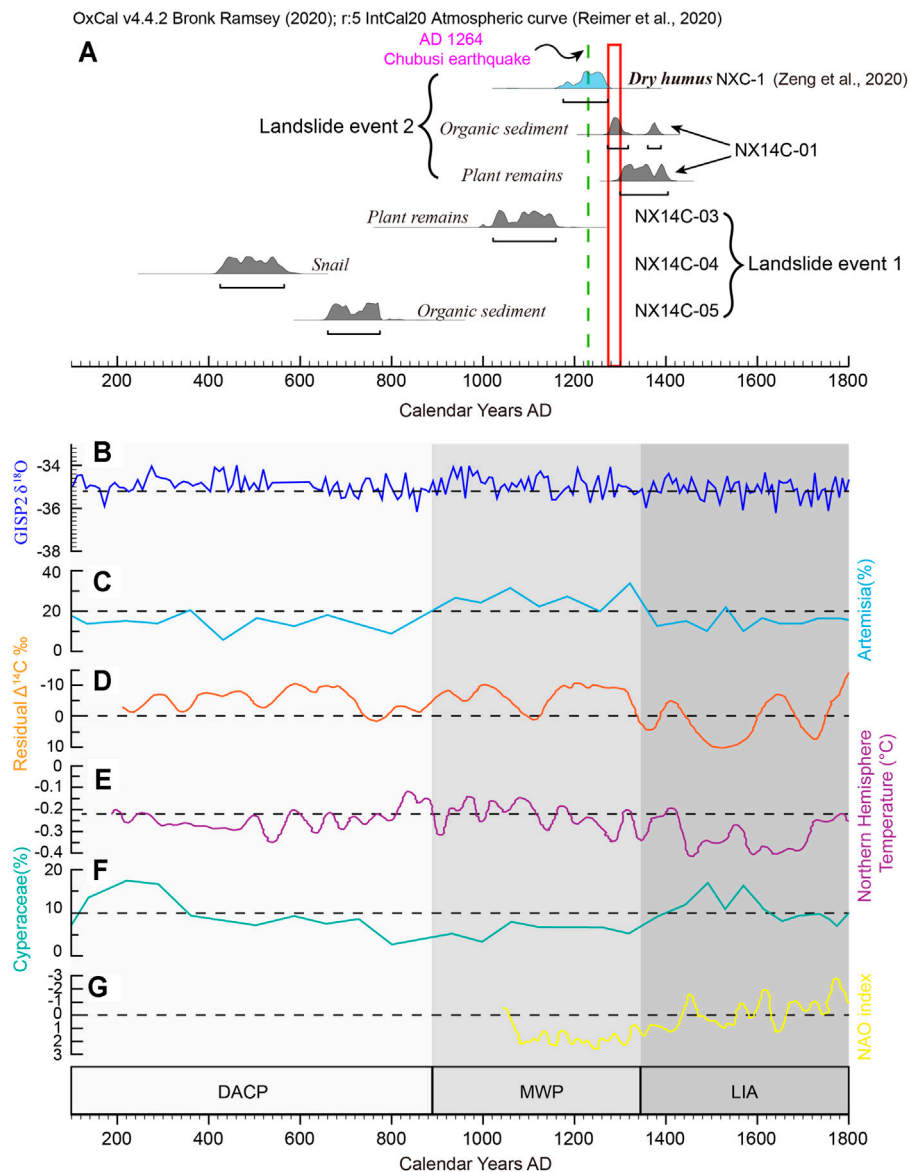
FIGURE 7 | (A) Two separate and distinct events occurred in the NCRA, **(C,F)** with the regional change in vegetation in the Yamzhog Yumco Lake area, southern Tibet and **(B,D,E,** and **G)** global environmental changes over the past 2,000 years. The **(C)** high percentage of *Artemisia* and **(F)** low percentage of *Cyperaceae* are indicative of the warm and dry climate period during the MWP (Guo et al., 2018). The environmental characteristics correspond with the **(B)** δ^{18}O records from the Greenland Ice Sheet Project 2 (Stuiver et al., 1995), **(D)** solar radiation records (Stuiver, 1998), **(E)** Northern Hemispheric temperature records (Mann and Jones, 2003), and **(G)** North Atlantic Oscillation (NAO) curves (Trouet et al., 2009). The green line is the 1264 AD Chubusi earthquake. The red rectangle shows the significant ^{14}C dating gap between the humus (Zeng et al., 2020) and plant remains sample in this study. DACP, Dark Age Cold Period; MWP, Medieval Warm Period; LIA, Little Ice Age.

temporal relationship between the age of the second landslide event and the 1264 AD Chubusi earthquake. The ^{14}C age of the humus from the peat sediment underlying the second landslide event is the maximum age, not the actual event age. That is, the maximum ^{14}C age cannot provide the dating precision necessary to connect the second event to the 1264 AD Chubusi earthquake. Although radiocarbon dating is one of the most widely used tools for dating landslides (Pánek, 2015), care is also required in interpreting these radiocarbon

ages. The ages of the samples gathered from different locations in the landslides provide different interpretations of the emplacement time of the landslide. For example, the ^{14}C age of the overlying lacustrine deposit indicates that the age of the Luanshibao landslide is 1,980 ± 30 years BP in the southeastern Tibetan Plateau (Guo et al., 2016). This age should be considered to be the minimum age. The 10Be exposure ages indicate that the Luanshibao landslide occurred at about 3,510 ± 346 years BP (Zeng et al., 2019).

In terrestrial cosmogenic nuclide surface exposure dating, the relatively unaltered upper surface (<5 cm) of a boulder is an ideal sample target (Lal, 1991; Gosse and Phillips, 2001). However, weathering, exhumation, or toppling of boulders may have occurred since the landslide emplacement (Dortch et al., 2009). The 10Be rock sample from the Luanshaibao landslide is characterized by weak weathering and no incomplete exposure due to toppling and covering of the boulders (Zeng et al., 2019). Thus, the 10Be exposure age may represent the lower age limit of the Luanshibao landslide. Compared with ^{14}C dating (Guo et al., 2016), the 10Be age is probably quite close to the actual emplacement age of the Luanshibao landslide. Although both ages attribute the trigger of the Luanshibao landslide to a seismic event (Guo et al., 2016; Zeng et al., 2019), the age variation causes different geological interpretations of the regional seismic shaking history. Similarly, relying solely on the upper age limit of the second landslide event of the NCRA emplacement is not sufficient to connect the event to the 1264 AD Chubusi earthquake (**Figure 7A**). In addition, our ^{14}C ages indicate that the second event of the NCRA occurred after 1,299–1,404 cal AD. The temporal connection between them suggests that the 1264 AD Chubusi earthquake is unlikely to be the trigger. The Angang fault represents a high seismogenic potential in the close field of the NCRA (Wu et al., 2015; Zeng et al., 2020), yet there are no paleoseismic records in the Angang graben as young as both landslide events that would corroborate a coseismic trigger during the past 2,000 years. However, the lack of a regional paleoseismicity record should not completely rule out a seismic trigger.

The continued activity on the Angang fault and the associated seismic events or regional earthquake-induced ground motion (e.g., the 1264 AD Chubusi earthquake) may have led to tectonic preconditioning of the occurrence of the NCRA. Wu et al. (2015) reported that the seismotectonic activity on the Angang fault has been ongoing since 2.6 ka BP, and the last vertical offset was approximately 2.8 and 6.1–7.9 m at the river terrace, which is equivalent to M_w 7 to 7.2 shallow seismic events. At least four strong earthquakes (≥M_w7) have occurred in the Angang graben since the Holocene, with a mean recurrence interval of 2.1 ka (Zeng et al., 2020). The normal fault is characterized by inherent structural complexity, resulting in a series of joints and fracture planes (Wang et al., 2019b). The continued activity on the normal fault may reduce the strength of the granite rock mass. The spatial distribution of the paleolandslides on both sides suggests the effect of tectonic weakening on the granite under the same climatic and lithological conditions. Ancient landslides have been identified in both sides of the Angang graben. However, the number of ancient landslides on the western side is larger than that on the eastern side (Wu et al., 2015). Twenty-one ancient landslides larger than 0.1 Mm^3 occurred in the Angang graben (Zeng et al., 2020), four of which occurred on the eastern side, while others are distributed along the Angang fault on the western side, within a distance of <1.5 km (Zeng et al., 2020).

In addition to seismic shaking, climate change can be assigned as a possible trigger of the NCRA. Fractures and fissures in the fault zone could have favored the penetration of water and led to increased weathering of the granite joints and increased pore pressure (Singeisen et al., 2020). This type of weakening and freeze–thaw cycle may have reduced the slope stability threshold and the effective friction on the sliding planes.

The sedimentary records from Yamzhog Yumco Lake show that the paleoclimate was warm–dry and cold–moist on the southern Tibetan Plateau over the past 2,000 years (Guo et al., 2018). The Little Ice Age (LIA, between ca.1300 and 1850 AD) and the Medieval Warm Period (MWP, between ca. 800 and 1300 AD) were the two most distinct climate anomalies (Hunt, 2006). The changes in the speleothem mineralogy record moister and/or cooler conditions associated with the onset of the LIA on the southern margin of the Tibetan Plateau (Denniston et al., 2000). Drier climatic conditions existed between 1000 and 1300 CE (MWP) on the southern Tibetan Plateau (Morrill et al., 2003). However, the precipitation was higher during the LIA than the MWP (He et al., 2013). Similar wetter conditions were recorded by lake sediments from Namco during the LIA compared with the MWP (Li et al., 2011). Overall, the warm and dry climate during the MWP shifted to low temperatures and relatively high moisture conditions during the LIA on the southern Tibetan Plateau (Guo et al., 2018). The second landslide event occurred during the climatic transition from the MWP to the LIA (**Figure 7**). Increased precipitation may have caused redistribution of the water and increased the pore water pressure (Aa et al., 2007). High precipitation events or wetter-than-normal periods lasting several months to years may cause failure of slopes (Johnson et al., 2017). Thus, the landslide may have been the result of these climatic effects acting on the fractured granite along the fault zone, which was preconditioned to failure by the continued activity on the western boundary fault of the Angang graben. In contrast, the first landslide event occurred in the Dark Age Cold Period (DACP), which has been reconstructed as cold and moist using the high-resolution palynological record from Yamzhog Yumco Lake (Guo et al., 2018). However, there were no significant distinct temperature and precipitation fluctuations (**Figure 7**). It remains uncertain whether the climatic change affected the occurrence of the first landslide event to a great extent.

However, it should be noted that the climate proxy only shows the change in the precipitation and temperature trends on the southern Tibetan Plateau (e.g., Guo et al., 2018). Further investigation through quantitative reconstruction of the magnitude of the past climate change is needed to support this suggestion.

Our results underscore the difficulty in accurately dating the NCRA using only ^{14}C dating. The low accuracy of the age determination results in a high uncertainty in identifying the actual trigger of the NCRA. Either climatic or seismic factors or both are likely to have caused the NCRA.

CONCLUSION

Plant remnants and snail shells were dated using ^{14}C dating to determine the age of the NCRA. Two landslide events were identified. The first event occurred before 425–565 cal AD, and the second event took place at 1,299–1,404 cal AD. The temporal correlation between the 1264 AD Chubusi earthquake and the NCRA suggests that there is no relationship between the events. However, the concomitant effect of crustal earthquakes on the rock avalanche initiation cannot be ruled out due to the regional seismotectonic setting. Similarly, climatic triggers cannot be easily ruled out because a long-lasting wetter climate may have led to the NCRA in the past 2,000 years. The low accuracy of the age determination makes it difficult to identify the actual trigger of the NCRA based solely on ^{14}C dating.

DATA AVAILABILITY STATEMENT

The original contributions presented in the study are included in the article/Supplementary Material. Further inquiries can be directed to the corresponding author.

REFERENCES

Aa, A. R., Sjåstad, J., Sønstegaard, E., and Blikra, L. H. (2007). Chronology of Holocene Rock-Avalanche Deposits Based on Schmidt-Hammer Relative Dating and Dust Stratigraphy in Nearby Bog Deposits, Vora, Inner Nordfjord, Norway. *Holocene* 17, 955–964. doi:10.1177/0959683607082411

Armijo, R., Tapponnier, P., Mercier, J. L., and Han, T.-L. (1986). Quaternary Extension in Southern Tibet: Field Observations and Tectonic Implications. *J. Geophys. Res.* 91, 13803–13872. doi:10.1029/JB091iB14p13803

Bowmanand Sheridan (1990). *Interpreting the Past. Radiocarbon Dating*. Los Angeles: University of California Press. doi:10.1029/JB091iB14p13803

Chung, S.-L., Chu, M.-F., Zhang, Y., Xie, Y., Lo, C.-H., Lee, T.-Y., et al. (2005). Tibetan Tectonic Evolution Inferred from Spatial and Temporal Variations in post-collisional Magmatism. *Earth-Science Rev.* 68, 173–196. doi:10.1016/j.earscirev.2004.05.001

Clague, J. J. (2015). "Paleolandslides," in *Landslide Hazards, Risks, and Disasters*. Boston: Academic Press, 321–344. doi:10.1016/B978-0-12-396452-6.00010-0

Denniston, R. F., González, L. A., Asmerom, Y., Sharma, R. H., and Reagan, M. K. (2000). Speleothem Evidence for Changes in Indian Summer Monsoon Precipitation over the Last ~2300 Years. *Quat. Res.* 53, 196–202. doi:10.1006/qres.1999.2111

Dortch, J. M., Owen, L. A., Haneberg, W. C., Caffee, M. W., Dietsch, C., and Kamp, U. (2009). Nature and Timing of Large Landslides in the Himalaya and Transhimalaya of Northern India. *Quat. Sci. Rev.* 28, 1037–1054. doi:10.1016/j.quascirev.2008.05.002

Gosse, J. C., and Phillips, F. M. (2001). Terrestrial *In Situ* Cosmogenic Nuclides: Theory and Application. *Quat. Sci. Rev.* 20, 1475–1560. doi:10.1016/S0277-3791(00)00171-2

Guo, C., Zhang, Y., Montgomery, D. R., Du, Y., Zhang, G., and Wang, S. (2016). How Unusual Is the Long-Runout of the Earthquake-Triggered Giant Luanshibao Landslide, Tibetan Plateau, China. *Geomorphology* 259, 145–154. doi:10.1016/j.geomorph.2016.02.013

Guo, C., Ma, Y., Meng, H., Hu, C., Li, D., Liu, J., et al. (2018). Changes in Vegetation and Environment in Yamzhog Yumco Lake on the Southern Tibetan Plateau over Past 2000 Years. *Palaeogeogr. Palaeoclimatol. Palaeoecol.* 501, 30–44. doi:10.1016/j.palaeo.2018.04.005

Ha, G., Wu, Z., and Liu, F. (2019). Late Quaternary Vertical Slip Rates along the Southern Yadong-Gulu Rift, Southern Tibetan Plateau. *Tectonophysics* 755, 75–90. doi:10.1016/j.tecto.2019.02.014

Harrison, T. M., Copeland, P., Kidd, W. S. F., and Lovera, O. M. (1995). Activation of the Nyainqentanghla Shear Zone: Implications for Uplift of the Southern Tibetan Plateau. *Tectonics* 14, 658–676. doi:10.1029/95TC00608

He, M., Yang, B., Bräuning, A., Wang, J., and Wang, Z. (2013). Tree-ring Derived Millennial Precipitation Record for the South-central Tibetan Plateau and its Possible Driving Mechanism. *Holocene* 23 (1), 36–45. doi:10.1177/0959683612450198

Hungr, O., Evans, S. G., Bovis, M. J., and Hutchinson, J. N. (2001). A Review of the Classification of Landslides of the Flow Typefication of Landslides of the Flow Type. *Environ. Eng. Geosci.* 7, 221–238. doi:10.2113/gseegeosci.7.3.221

Hunt, B. G. (2006). The Medieval Warm Period, the Little Ice Age and Simulated Climatic Variability. *Clim. Dyn.* 27, 677–694. doi:10.1007/s00382-006-0153-5

Ji, W.-Q., Wu, F.-Y., Chung, S.-L., Li, J.-X., and Liu, C.-Z. (2009). Zircon U–Pb Geochronology and Hf Isotopic Constraints on Petrogenesis of the Gangdese Batholith, Southern Tibet. *Chem. Geol.* 262, 229–245. doi:10.1016/j.chemgeo.2009.01.020

Jibson, R. W. (2009). Chapter 8 Using Landslides for Paleoseismic Analysis. *Int. Geophys.* 95, 565–601. doi:10.1016/S0013-7952(96)00039-710.1016/s0074-6142(09)95008-2

Johnson, B. G., Smith, J. A., and Diemer, J. A. (2017). A Chronology of post-glacial Landslides Suggests that Slight Increases in Precipitation Could Trigger a Disproportionate Geomorphic Response. *Earth Surf. Process. Landforms* 42, 2223–2239. doi:10.1002/esp.4168

Kilian, M. R., Van Der Plicht, J., and Van Geel, B. (1995). Dating raised bogs: New aspects of AMS 14C wiggle matching, a reservoir effect and climatic change. *Quaternary Science Reviews* 14, 959–966. doi:10.1016/0277-3791(95)00081-X

Korup, O., Schneider, D., Huggel, C., and Dufresne, A. (2013). "7.18 Long-Runout Landslides," in *Treatise on Geomorphology*. San Diego: Academic Press, 183–199. doi:10.1016/B978-0-12-374739-6.00164-0

Lal, D. (1991). Cosmic ray Labeling of Erosion Surfaces: *In Situ* Nuclide Production Rates and Erosion Models. *Earth Planet. Sci. Lett.* 104, 424–439. doi:10.1016/0012-821X(91)90220-C

AUTHOR CONTRIBUTIONS

FL conceived the idea of the study. FL, GH, and MC performed the field work. GH and MC prepared the samples and conducted the experiments. FL, GH, MC, XY, and LL conducted the discussion. FL interpreted the data and wrote the paper. GH and JP improved the figures. All authors contributed to the revision of the text.

FUNDING

ACKNOWLEDGMENTS

Lang, A., Moya, J., Corominas, J., Schrott, L., and Dikau, R. (1999). Classic and new dating methods for assessing the temporal occurrence of mass movements. *Geomorphology* 30, 33–52. doi:10.1016/S0169-555X(99)00043-4

Li, Q., Lu, H., Zhu, L., Wu, N., Wang, J., and Lu, X. (2011). Pollen-inferred Climate Changes and Vertical Shifts of alpine Vegetation Belts on the Northern Slope of the Nyainqentanglha Mountains (central Tibetan Plateau) since 8.4 Kyr BP. *Holocene* 21, 939–950. doi:10.1177/0959683611400218

Ma, C., Zhu, C., Zheng, C., Yin, Q., and Zhao, Z. (2009). Climate Changes in East China since the Late-Glacial Inferred from High-Resolution Mountain Peat Humification Records. *Sci. China Ser. D-Earth Sci.* 52, 118–131. doi:10.1007/s11430-009-0003-5

Mann, M. E., and Jones, P. D. (2003). Global surface temperatures over the past two millennia. *Geophys. Res. Lett* 30. doi:10.1029/2003GL017814

Maheo, G., Leloup, P., Valli, F., Lacassin, R., Arnaud, N., Paquette, J., et al. (2007). Post 4 Ma Initiation of normal Faulting in Southern Tibet. Constraints from the Kung Co Half Graben. *Earth Planet. Sci. Lett.* 256, 233–243. doi:10.1016/j.epsl.2007.01.029

Mitchell, W. A., McSaveney, M. J., Zondervan, A., Kim, K., Dunning, S. A., and Taylor, P. J. (2007). The Keylong Serai Rock Avalanche, NW Indian Himalaya: Geomorphology and Palaeoseismic Implications. *Landslides* 4, 245–254. doi:10.1007/s10346-007-0085-0

Morrill, C., Overpeck, J. T., and Cole, J. E. (2003). A Synthesis of Abrupt Changes in the Asian Summer Monsoon since the Last Deglaciation. *Holocene* 13, 465–476. doi:10.1191/0959683603hl639ft

Nilsson, M., Klarqvist, M., Bohlin, E., and Possnert, G. (2001). Variation in 14C Age of Macrofossils and Different Fractions of Minute Peat Samples Dated by AMS. *Holocene* 11, 579–586. doi:10.1191/095968301680223521

Pánek, T., Korup, O., Minár, J., and Hradecký, J. (2016). Giant Landslides and Highstands of the Caspian Sea. *Geology* 44, 939–942. doi:10.1130/G38259.1

Pánek, T. (2015). Recent Progress in Landslide Dating. *Prog. Phys. Geogr. Earth Environ.* 39, 168–198. doi:10.1177/0309133314550671

Piotrowska, N., Blaauw, M., Mauquoy, D., and Chambers, F. M. (2011). Constructing Deposition Chronologies for Peat Deposits Using Radiocarbon Dating. *Mires Peat* 7, 1–14.

Reimer, P. J., Austin, W. E. N., Bard, E., Bayliss, A., Blackwell, P. G., Bronk Ramsey, C., et al. (2020). The IntCal20 Northern Hemisphere Radiocarbon Age Calibration Curve (0-55 Cal kBP). *Radiocarbon* 62, 725–757. doi:10.1017/RDC.2020.41

Sembroni, A., Molin, P., Refice, A., and Messina, A. (2019). Evolution of a Hillslope by Rock Avalanches: Insights from Analog Models. *Landslides* 16, 1841–1853. doi:10.1007/s10346-019-01229-0

Shore, J. S., Bartley, D. D., and Harkness, D. D. (1995). Problems encountered with the 14C dating of peat. *Quaternary Science Reviews* 14, 373–383. doi:10.1016/0277-3791(95)00031-3

Singeisen, C., Ivy-Ochs, S., Wolter, A., Steinemann, O., Akçar, N., Yesilyurt, S., et al. (2020). The Kandersteg Rock Avalanche (Switzerland): Integrated Analysis of a Late Holocene Catastrophic Event. *Landslides* 17, 1297–1317. doi:10.1007/s10346-020-01365-y

Struble, W. T., Roering, J. J., Black, B. A., Burns, W. J., Calhoun, N., and Wetherell, L. (2020). Dendrochronological Dating of Landslides in Western Oregon: Searching for Signals of the Cascadia A.D. 1700 Earthquake. *GSA Bull.* 132, 1775–1791. doi:10.1130/B35269.1

Stuiver, M., Grootes, P. M., and Braziunas, T. F. (1995). The GISP2 δ18O Climate Record of the Past 16,500 Years and the Role of the Sun, Ocean, and Volcanoes. *Quaternary Research* 44, 341–354. doi:10.1006/qres.1995.1079

Stuiver, M., Reimer, P. J., Bard, E., Beck, J. W., Burr, G. S., and Hughen, K. A. (1998). INTCAL98 radiocarbon age calibration, 24,000-0 cal BP. *Radiocarbon* 40, 1041–1083. doi:10.1017/S0033822200019123

Trouet, V., Esper, J., Graham, N. E., Baker, A., Scourse, J. D., and Frank, D. C. (2009). Persistent Positive North Atlantic Oscillation Mode Dominated the Medieval Climate Anomaly. *Science* 324, 78–80. doi:10.1126/science.1166349

Wang, Y.-F., Cheng, Q.-G., Shi, A.-W., Yuan, Y.-Q., Yin, B.-M., and Qiu, Y.-H. (2019a). Sedimentary Deformation Structures in the Nyixoi Chongco Rock Avalanche: Implications on Rock Avalanche Transport Mechanisms. *Landslides* 16, 523–532. doi:10.1007/s10346-018-1117-7

Wang, Y.-F., Cheng, Q.-G., Shi, A.-W., Yuan, Y.-Q., Qiu, Y.-H., and Yin, B.-M. (2019b). Characteristics and Transport Mechanism of the Nyixoi Chongco Rock Avalanche on the Tibetan Plateau, China. *Geomorphology* 343, 92–105. doi:10.1016/j.geomorph.2019.07.002

Wu, Z. H., Ye, P. S., Wang, C. M., Zhang, K. Q., Zhao, H., Zheng, Y. G., et al. (2015). The Relics, Ages, and Significance of Prehistoric Large Earthquakes in the Angang Graben in South Tibet. *Earth Sci. J. China Uni. Geosci.* 40, 1621–1642. (In Chinese with English abstract). doi:10.3799/dqkx.2015.147

Yin, A., and Harrison, T. M. (2000). Geologic Evolution of the Himalayan-Tibetan Orogen. *Annu. Rev. Earth Planet. Sci.* 28, 211–280. doi:10.1146/annurev.earth.28.1.211

Zeng, Q., Yuan, G., Davies, T., Xu, B., Wei, R., Xue, X., et al. (2019). 10 Be Dating and Seismic Origin of Luanshibao Rock Avalanche in SE Tibetan Plateau and Implications on Litang Active Fault. *Landslides* 17, 1–14. doi:10.1007/s10346-019-01319-z

Zeng, Q., Yuan, G., McSaveney, M., Ma, F., Wei, R., Liao, L., et al. (2020). Timing and Seismic Origin of Nixu Rock Avalanche in Southern Tibet and its Implications on Nimu Active Fault. *Eng. Geol.* 268, 105522. doi:10.1016/j.enggeo.2020.105522

Zhou, W., Liu, X. F., and Wu, Z. K. (2002). Peat Record Reflecting Holocene Climatic Change in the Zoig Plateau and AMS Radiocarbon Dating. *Chin. Sci Bull* 47 (1), 66–70. doi:10.1360/02tb9013

Zimmerman, S., and Myrbo, A. (2015). "Lacustrine Environments (14C)," in *Encyclopedia of Earth Sciences Series* (Netherlands: Springer), 365–371. doi:10.1007/978-94-007-6304-3_160